Available online at www.sciencedirect.com
SCIENCE DIRECT
Journal of Fluorine Chemistry 125 (2004) 1663–1670
JOURNAL OF FLUORINE CHEMISTRY
www.elsevier.com/locate/fluor

Synthesis, vibrational and NMR spectroscopic characterization of $[N(CH_3)_4][IO_2F_2]$ and X-ray crystal structure of $[N(CH_3)_4]_2[IO_2F_2][HF_2]$

Michael Gerken[a,b,*], Johnathan P. Mack[a], Gary J. Schrobilgen[b,*], Reijo J. Suontamo[c]

[a]*Department of Chemistry and Biochemistry, University of Lethbridge, Lethbridge, AB T1K 3M4, Canada*
[b]*Department of Chemistry, McMaster University, Hamilton, ON L8S 4M1, Canada*
[c]*Department of Chemistry, University of Jyväskylä, P.O. Box 35, FIN-40014 Jyväskylä, Finland*

Available online 14 October 2004

Abstract

The salt, $[N(CH_3)_4][IO_2F_2]$, was prepared from $[N(CH_3)_4][IO_3]$ and 49% aqueous HF, and characterized by Raman, infrared, and ^{19}F NMR spectroscopy. Crystals of $[N(CH_3)_4]_2[IO_2F_2][HF_2]$ were obtained by reduction of $[N(CH_3)_4][cis\text{-}IO_2F_4]$ in the presence of $[N(CH_3)_4][F]$ in CH_3CN solvent and were characterized by Raman spectroscopy and single-crystal X-ray diffraction: *C2/m*, a = 14.6765(2) Å, b = 8.60490(10) Å, c = 13.9572(2) Å, β = 120.2040(10)°, V = 1523.35(3) Å^3, Z = 4 and R = 0.0192 at 210 K. The crystal structure consists of two $IO_2F_2^-$ anions that are symmetrically bridged by two HF_2^- anions, forming a $[F_2O_2I(FHF)_2IO_2F_2]^{4-}$ dimer. The symmetric bridging coordination for the HF_2^- anion in this structure represents a new bonding modality for the bifluoride anion.

Keywords: Iodine oxide fluorides; Difluoroiodate; Bifluoride; X-ray crystallography; Vibrational spectroscopy; ^{19}F NMR spectroscopy

1. Introduction

The IO_3^- and IO_4^- anions undergo solvolysis in aqueous and anhydrous HF, with the degree of fluorination depending on the formal oxidation state of iodine and on the HF concentration. The reaction of IO_4^- with excess anhydrous HF produces a kinetically controlled mixture of the *cis*-$IO_2F_4^-$ and *trans*-$IO_2F_4^-$ anions (Eq. (1)) [1,2], whereas the reaction of IO_3^- with anhydrous HF results in the complete replacement of all oxygen ligand atoms by fluorine atoms, yielding IF_5 (Eq. (2)) [3]. The use of aqueous HF solutions

$$[N(CH_3)_4][IO_4] + 4HF \rightarrow [N(CH_3)]_4[IO_2F_4] + 2H_2O \quad (1)$$

$$[Na][IO_3] + 7HF \rightarrow [Na(HF_2)] + IF_5 + 3H_2O \quad (2)$$

(40%) for the fluorination of alkali metal iodates leads to the exclusive formation of the $IO_2F_2^-$ salt according to Eq. (3) [4] and has led to the isolation of the Na^+ [4], K^+ [4],

$$[M][IO_3] + 2HF_{(aq)} \rightarrow [M][IO_2F_2]_{(aq)} + H_2O_{(l)}, \quad M = Li^+, Na^+, K^+, Cs^+ \text{ and } NH_4^+ \quad (3)$$

Rb^+ [4], Cs^+ [4,5] and NH_4^+ [4] salts. In contrast, $[Ag][IO_2F_2]$ has been prepared by solvolysis of $[Ag][IO_3]$ in anhydrous HF [6]. The majority of difluoroiodates have been poorly characterized and only $[K][IO_2F_2]$, which has been shown to be ferroelastic at room temperature, has been characterized by X-ray crystallography [7,8] and by Raman and infrared spectroscopy [9,10]. The Cs^+ salt could not be prepared pure, but was isolated as $[Cs][IO_2F_2]\cdot(1/3)H_2O$ [11] and as a mixture of $[Cs][IO_2F_2]$ and $[Cs][IOF_4]$ [5].

The present paper reports the syntheses and characterizations of $[N(CH_3)_4][IO_2F_2]$ and the double salt, $[N(CH_3)_4]_2[IO_2F_2][HF_2]$, which are the first $N(CH_3)_4^+$ salts of $IO_2F_2^-$. The latter salt, which contains bridging HF_2^- ions, represents a unique coordination mode for the HF_2^- ion.

* Corresponding authors. Tel.: +1 403 329 2173 (M. Gerken)/+1 905 525 9140x23306 (G.J. Schrobilgen); fax: +1 403 329 2057 (M. Gerken)/+1 905 522 2509 (G.J. Schrobilgen).
E-mail addresses: michael.gerken@uleth.ca (M. Gerken), schrobil@mcmaster.ca (G.J. Schrobilgen).

0022-1139/$ – see front matter © 2004 Elsevier B.V. All rights reserved.
doi:10.1016/j.jfluchem.2004.09.005

2. Results and discussion

2.1. Synthesis of $[N(CH_3)_4][IO_2F_2]$ and ^{19}F NMR spectroscopic characterization

The $N(CH_3)_4^+$ salt of the difluoroiodate anion, $IO_2F_2^-$, was prepared by solvolysis of $[N(CH_3)_4][IO_3]$ in excess 49% aqueous HF according to Eq. (4). The $[N(CH_3)_4][IO_2F_2]$

$$[N(CH_3)_4][IO_3] + 2HF_{(aq)} \rightarrow [N(CH_3)_4][IO_2F_2]_{(aq)} + H_2O_{(l)} \quad (4)$$

salt has a high solubility in aqueous HF and only a microcrystalline precipitate forms at high concentrations as an HF solvate, $[N(CH_3)_4][IO_2F_2]\cdot nHF$, which was identified by Raman spectroscopy [12]. The HF solvent molecules can be removed under dynamic vacuum at 80 °C to give pure $[N(CH_3)_4][IO_2F_2]$. The room-temperature ^{19}F NMR spectrum of anhydrous and HF-free $[N(CH_3)_4][IO_2F_2]$ in CH_3CN, which is sparingly soluble in CH_3CN at room temperature, showed a singlet at 13.7 ppm. The ^{19}F chemical shift of $IO_2F_2^-$ is in the range characteristic of iodine(V) fluorine compounds, as exemplified by the ^{19}F chemical shifts of IOF_4^- (3–9 ppm, depending on the cation) and IOF_3 (13 ppm) in CH_3CN [13].

2.2. Formation of $[N(CH_3)_4]_2[IO_2F_2][HF_2]$

Attempts to grow crystals of $[N(CH_3)_4][cis\text{-}IO_2F_4]$ [14] at ambient temperature from CH_3CN solvent in the presence of $[N(CH_3)_4][F]$ yielded colorless crystals of $[N(CH_3)_4]_2[IO_2F_2][HF_2]$ instead. Although the oxidation products have not been identified, $[N(CH_3)_4][F]$ apparently plays a crucial role in the reduction of $IO_2F_4^-$ to $IO_2F_2^-$. At room temperature, anhydrous $[N(CH_3)_4][F]$ abstracts H^+ from CH_3CN solvent yielding the CH_2CN^- anion [15], which likely serves as a reducing agent towards $IO_2F_4^-$.

2.3. Vibrational spectroscopic characterization

2.3.1. $[N(CH_3)_4][IO_2F_2]$

The $[N(CH_3)_4][IO_2F_2]$ salt was characterized by low-temperature Raman spectroscopy and room-temperature infrared spectroscopy. The Raman and infrared spectra are shown in Fig. 1 and the experimental vibrational frequencies of $[N(CH_3)_4][IO_2F_2]$ are listed in Table 1 together with the calculated vibrational frequencies of the $IO_2F_2^-$ anion and their assignments.

The vibrations of the $IO_2F_2^-$ anion span the irreducible representations $\Gamma = 4A_1 + A_2 + 2B_1 + 2B_2$ under C_{2v} point symmetry (for IO_2 in the yz-plane). While all modes are Raman-active, the A_1, B_1 and B_2 modes are infrared-active and the A_2 mode is infrared-inactive. The vibrational frequencies of the $IO_2F_2^-$ anion in $[N(CH_3)_4][IO_2F_2]$ are in good agreement with those reported for $[K][IO_2F_2]$ [9,10], however, fewer anion bands are observed in the $N(CH_3)_4^+$ salt. The additional signals that were reported for $[K][IO_2F_2]$ are likely attributable to impurities. Assignments of the vibrational bands for the $IO_2F_2^-$ anion are based on the calculated frequencies (see Section 2.5) and the observed intensities. The spectra of $[N(CH_3)_4][IO_2F_2]$ are dominated by the symmetric and antisymmetric IO_2 stretching bands at 818 and 849 cm^{-1}, respectively. As a result of the nearly linear IF_2 arrangement, the symmetric IF_2 stretch is observed as a strong Raman band at 467 cm^{-1} and as a weak shoulder in the infrared spectrum at 468 cm^{-1}, and the antisymmetric IF_2 stretch is observed as a very strong infrared band at 445 cm^{-1} which does not appear in the Raman spectrum.

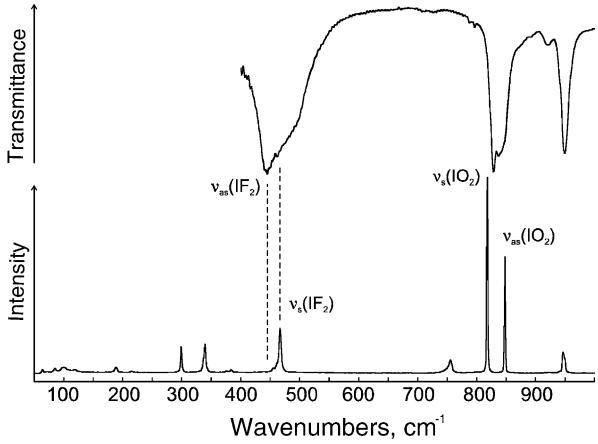

Fig. 1. The vibrational spectra of $[N(CH_3)_4][IO_2F_2]$: (a) Raman spectrum (lower trace) recorded at −100 °C in a glass tube using 1064 nm excitation and (b) infrared spectrum (upper trace) recorded at room temperature in an AgCl pellet.

2.3.2. $[N(CH_3)_4]_2[IO_2F_2][HF_2]$

The Raman spectrum of the single crystal used for the X-ray crystal structure determination of $[N(CH_3)_4]_2[IO_2F_2][HF_2]$ (Section 2.4) was recorded at room temperature (Fig. 2). Changing the orientation of the crystal did not result in noticeable changes in the intensities or positions of the Raman bands. The frequencies and their assignments are listed in Table 2. The assignments for the Raman bands of the $IO_2F_2^-$ anion are based on those given for $[N(CH_3)_4][IO_2F_2]$ in Table 1.

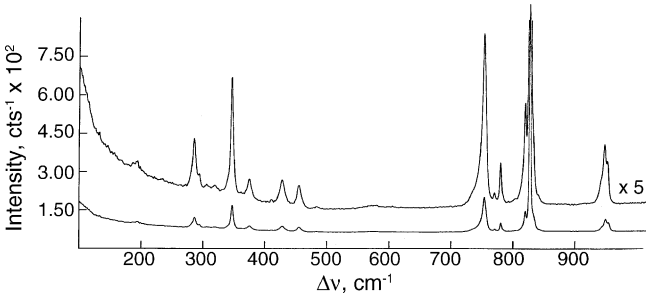

Fig. 2. The Raman spectrum of a single crystal of $[N(CH_3)_4]_2[IO_2F_2][HF_2]$ recorded in a glass Lindemann capillary at room temperature using 514.5 nm excitation.

Table 1
Experimental vibrational frequencies and assignments for $[N(CH_3)_4][IO_2F_2]$ and $[K][IO_2F_2]$ and calculated vibrational frequencies for $IO_2F_2^-$

Frequency[a] (cm^{-1})						Assignment $IO_2F_2^-$ (C_{2v})
$[N(CH_3)_4][IO_2F_2]$		$[K][IO_2F_2]$[d]		Calculated frequencies[e]		
Raman[b]	Infrared[c]	Raman	Infrared	MP2	SVWN	
849(59)	844 sh	838 w	851 m	907(266) [7]	821(145)	$\nu_8(B_2)$, $\nu_{as}(IO_2)$
	837 s		845 m			
818(100)	829 vs	817 vs	819 vs	918(64) [33]	792(33)	$\nu_1(A_1)$, $\nu_s(IO_2)$
		804 w, sh	805 w, sh			
	493 sh					
467(23)	468 sh	479 s	485 vs	425(8) [27]	447(4)	$\nu_2(A_1)$, $\nu_s(IF_2)$
	445 vs	456 vw	440 m	453(413) [0]	498(282)	$\nu_6(B_1)$, $\nu_{as}(IF_2)$
			407 m			
		360 m	360 s			
			351 w, sh			
339(15)		346 w	345 s	319(46) [5]	283(38)	$\nu_3(A_1)$, $\delta_s(IO_2)$
299(13)		323 s		289(1) [2]	266(8)	$\nu_7(B_1)$, $\delta_{rocking}(IF_2)$
215(1)			220 m, sh	254(0) [4]	233(0)	$\nu_5(A_2)$, torsion
				165(20) [<0.5]	160(14)	$\nu_9(B_2)$, $\delta_{wagging}(IF_2)$
188(3)		194 vw	197 s	144(11) [1]	140(4)	$\nu_4(A_1)$, $\delta_s(IF_2)$
118(2)						Lattice modes
99(3)						
84(2)						

[a] Abbreviations denote shoulder (sh), very strong (vs), strong (s), medium (m), weak (w), very weak (vw), and broad (br).
[b] The $N(CH_3)_4^+$ cation modes were observed in the Raman spectrum (−100 °C) at 376(1), 384(1), $\nu_8(E)$; 456(2), $\nu_{19}(T_2)$; 756(7), $\nu_3(A_1)$; 942 sh, 947(10), 950 sh, $\nu_{18}(T_2)$; 1174(1), 1179(2), $\nu_7(E)$; 1292(1), $\nu_{17}(T_2)$; 1398(2), 1405(2), 1409(1), $\nu_{16}(T_2)$; 1457(1), 1469(16), 1474(14), $\nu_2(A_1)$, $\nu_6(E)$; 2788(2), 2804(1), 2807(1), 2899(1) 2907(1), 2960(8), 2975 sh, 2990(2), 3001(2), 3032(6), 3037(5), 3043(8), 3059(7) cm^{-1}, $\nu(CH_3)$ and binary bands [15,16].
[c] The $N(CH_3)_4^+$ cation modes were observed in the infrared spectrum at 922 w, 949 s, $\nu_{18}(T_2)$; 1063 vw, 1182 vw, 1199 vw, $\nu_7(E)$; 1240 w, 1290 w, $\nu_{17}(T_2)$; 1402 m, 1411 m, $\nu_{16}(T_2)$; 1450 w, 1468 w, 1486 s, 1493 s, $\nu_2(A_1)$, $\nu_6(E)$; 1783 br vw, 2042 vw, 2161 vw, 2237 vw, 2349 w, 2480 w, 2515 w, 22575 w, 2619 vw, 2697 vw, 2747w, 2793 w, 2852 w, 2923 w, 2969 w, 3043 m, 3056 m, 3099 w, 3135 w, 3416 w, 3495 w cm^{-1}, $\nu(CH_3)$ and binary bands [15,16].
[d] Values are from [10].
[e] Infrared intensities, in km mol^{-1} are given in parentheses, unscaled Raman intensities in $Å^4$ amu^{-1} are given in square brackets.

The band at 832 cm^{-1} is assigned to the symmetric I–O stretch $\nu_1(A_1)$, which is shifted 20 cm^{-1} to higher frequency with respect to $\nu_s(IO_2)$ in $[N(CH_3)_4][IO_2F_2]$ (818 cm^{-1}). The symmetric and antisymmetric IF_2 stretching modes were assigned to the bands at 430 and 413 cm^{-1}, respectively. The IF_2 stretching frequencies of $[N(CH_3)_4]_2[IO_2F_2][HF_2]$ appear at significantly lower frequency than those of $[N(CH_3)_4][IO_2F_2]$. The weak band at 581 cm^{-1} is assigned to the symmetric stretch of the bifluoride ion, which is slightly lower in frequency than that in $[N(CH_3)_4][HF_2]$ (596 cm^{-1}) [17] and consistent with the strong I···F contacts in the crystal structure (see Section 2.4).

2.4. X-ray crystal structure of $[N(CH_3)_4]_2[IO_2F_2][HF_2]$

Details of the data collection parameters and other crystallographic information for $[N(CH_3)_4]_2[IO_2F_2][HF_2]$ are given in Table 3. Important bond lengths, angles and contacts for $[N(CH_3)_4]_2[IO_2F_2][HF_2]$ are listed in Table 4.

The crystal structure of $[N(CH_3)_4]_2[IO_2F_2][HF_2]$ contains alternating layers of $N(CH_3)_4^+$ cations and $IO_2F_2^-$ and HF_2^- anions in the (1 0 −1) plane (Fig. 3). The two crystallographically independent $N(CH_3)_4^+$ cations, which are tetrahedral about the nitrogen atom to within $\pm 3\sigma$ and have the expected bond lengths, are not discussed further. Strong contacts occurring between two $IO_2F_2^-$ and two HF_2^- anions lying in the IO_2-planes of the crystallographically equivalent $IO_2F_2^-$ anions give rise to bifluoride ion-bridged $[F_2O_2I(FHF)_2IO_2F_2]^{4-}$ dimers (Fig. 3). The I–O (1.774(2) Å) and I–F (2.025(2), 2.027(2) Å) bond lengths for $IO_2F_2^-$ anion in $[N(CH_3)_4]_2[IO_2F_2][HF_2]$ are in good agreement with those previously reported for the crystal structure of $[K][IO_2F_2]$ (I–O: 1.762(8), 1.775(13) Å; I–F: 2.015(8), 1.985(8) Å) [8]. As in the structure of the K^+ salt, the two fluorine atoms of each $IO_2F_2^-$ anion occupy axial positions, while the two oxygen atoms and the lone pair are in the equatorial plane, as predicted by the VSEPR rules for an AX_2Y_2E arrangement of bond-pair and lone-pair domains [18]. The axial F–I–F angle is slightly bent (176.73(8)°) towards the lone-pair position, away from the two I–O double bond domains, and contrasts with the essentially linear F–I–F arrangement (179.1(5)°) in the K^+ salt [8]. The bending of the axial ligands in the pseudo-trigonal bipyramidal AX_2Y_2E structures towards the lone-pair position has also been found in the crystal structures of XeO_2F_2 (174.7(4)°) [19], $XeO_2F_2{\cdot}TcO_2F_3$ (175.7(6)°) [20], and $XeO_2(OTeF_5)_2$ (163.7(2)°) [21], and, in the case of XeO_2F_2, has been attributed to a non-spherical charge distribution of the lone pair, which is more extended in the equatorial plane and seems to reduce the repulsive

Table 2
Experimental vibrational frequencies and assignments for $[N(CH_3)_4]_2[IO_2F_2][HF_2]$

Raman frequency (cm^{-1})[a]	Assignments		
	$IO_2F_2^-$ (C_{2v})	$N(CH_3)_4^+$ (T_d)	HF_2^- ($D_{\infty h}$)
3041 sh			
3034(14)			
3020(19)			
2968(16)		$\nu(CH_3)$ and binary bands	
2933(13)			
2897(7)			
2837(11)			
1479(24)			
1473 sh		$\nu_6(E)$, $\nu_2(A_1)$	
1420(1)		$\nu_{16}(T_2)$	
1293(1)		$\nu_{17}(T_2)$	
1189(2)		$\nu_7(E)$	
960(4)			
955(6)		$\nu_{18}(T_2)$	
950 sh			
847(1)			
838 sh			
832(100)	$\nu_1(A_1)$, $\nu_s(IO_2)$		
825(9)	$\nu_8(B_2)$, $\nu_{as}(IO_2)$		
811(<0.5)			
758(16)		$\nu_3(A_1)$	
741 sh			
581(<0.5)			$\nu_1(\Sigma_g^+)$
487(<0.5)			
458(1)		$\nu_{19}(T_2)$	
430(3)	$\nu_2(A_1)$, $\nu_s(IF_2)$		
413(<0.5)	$\nu_6(B_1)$, $\nu_{as}(IF_2)$		
378(2)		$\nu_8(E)$	
349(10)	$\nu_3(A_1)$, $\delta_s(IO_2)$		
344 sh			
321(1)			
288(5)	$\nu_7(B_1)$, $\delta_{rocking}(IO_2)$		
197(1)	$\nu_4(A_1)$, $\delta_s(IF_2)$		

[a] The Raman spectrum was recorded on a single crystal inside a glass Lindemann capillary at room temperature using 514.5 nm excitation. Values in parentheses denote relative Raman intensities; and sh a shoulder. Weak IO_3^- bands, resulting from surface hydrolysis, were observed at 296(1), 308(1), 775(1) and 785(4) cm^{-1} [12].

interactions between the lone pair and the axial ligands [22]. The axial F–I–F angle in $IO_2F_2^-$ is, however, significantly greater than the corresponding F–Xe–F angles in the neutral xenon analogues, reflecting the decreased steric demands of O–I double bonds, which are more polar in an anion. The smaller I–O bond domain in $IO_2F_2^-$ also results in smaller O–I–O bond angles in $[N(CH_3)_4]_2[IO_2F_2][HF_2]$ (101.98(12)°) and $[K][IO_2F_2]$ (102.0(6)°) [8] when compared with those in XeO_2F_2 (105.7(3)°) [19], $XeO_2F_2 \cdot TcO_2F_3$ (105.6(6)°) [20], and $XeO_2(OTeF_5)_2$ (106.5(2)°) [21]. The increased bond polarity in an anionic species is also reflected in the longer I–O and I–F bond lengths in the $IO_2F_2^-$ anion when compared with the Xe–O (1.714(4) Å) and Xe–F (1.899(3) Å) bond lengths of XeO_2F_2 [19].

The two fluorine atoms of the HF_2^- anion are related through a crystallographic two-fold axis and the hydrogen

Table 3
Summary of crystal data and refinement results for $[N(CH_3)_4]_2[IO_2F_2][HF_2]$

	$[N(CH_3)_4]_2[IO_2F_2][HF_2]$
Formula	$C_8H_{25}F_4IN_2O_2$
Space group	*C*2/*m* (No. 12)
a (Å)	14.6765(2)
b (Å)	8.60490(10)
c (Å)	13.9572(2)
α (°)	90
β (°)	120.2040(10)
γ (°)	90
V (Å^3)	1523.35(3)
Z (molecules/unit cell)	4
Molecular weight	384.20
Calcd. density (g cm^{-3})	1.675
R_1[a]	0.0192
wR_2[b]	0.0455

[a] $R_1 = \sum |F_0| - |F_c| / \sum |F_0|$.
[b] $wR_2 = \sum |(|F_0| - |F_c|)w^{1/2}| / \sum (|F_0|w)$ where $w = 1/[\sigma^2(F) + (0.0344)^2 + 4.94]$.

atom was refined on the special position (2). The F(3)···F(3A) distance (2.277(5) Å) is somewhat longer than that in the crystal structure of $[N(CH_3)_4][HF_2]$ (2.213(4) Å) and is very similar to that in $[K][HF_2]$ (2.277(6) Å) [17]. The F···F distance in the present structure is significantly shorter than those found in transition-metal complexes having terminal (FHF) moieties: $[Ni(F\cdots HF)(C_4N_2F_2H)(PEt_3)_2]$ (2.400(6) Å) [23], $Mo(PMe_3)_4(H)_2F(F\cdots HF)$ (2.351(8) Å) [24], $W(PMe_3)_4(H)_2F(F\cdots HF)$ (2.389(6) Å) [25], *trans*-$Pd(PPh_3)_2Me(F\cdots HF)$ (2.31 Å) [26]. Hence, the FHF moieties in the aforementioned transition-metal complexes are best described as HF molecules hydrogen-bonded to fluorine ligands, which is supported by ^{19}F and ^1H NMR spectroscopic studies of these complexes [23–26]. The F···F distance in *trans*-$Ru(dmpe)_2(H)(F\cdots HF)$ of 2.286(8) Å is close to that of ionic bifluoride, however, ^1H and ^{19}F NMR spectroscopic results favor a hydrogen-bonded description [27]. The number of structurally characterized compounds containing bridging hydrogen fluoride molecules is limited to the dimeric niobium and osmium species, $[(\eta^5\text{-}C_5Me_5)NbF_4(HF)AsF_3]_2$ [28], $[OsO_3F(HF)_2AsF_6]_2$ and to polymeric $[OsO_3F(HF)SbF_6]$ [29]. With F···F distances of 2.686 Å (Nb) and between 2.429(8) and 2.518(9) Å (Os), these structures contain bridging hydrogen-bonded HF solvent molecules, which contrast with the symmetric bridging coordination mode of HF_2^- in the crystal structure of $[N(CH_3)_4]_2[IO_2F_2][HF_2]$.

The $IO_2F_2^-$ and HF_2^- anions in the $[F_2O_2I(FHF)_2IO_2F_2]^{4-}$ dimer exhibit short F···I contacts (2.806(2) Å) when compared with the sum of the fluorine and iodine van der Waal's radii (3.46 [30] and 3.50 Å [31]), with both bifluoride anions symmetrically bridging two $IO_2F_2^-$ anions. The fluorine atoms of two symmetry-related bifluoride ions coordinate to both iodine atoms, avoiding the iodine lone-pair positions, resulting in pseudo-octahedral coordination spheres for the iodine atoms. A similar extension of the

Table 4
Experimental metric parameters for $[N(CH_3)_4]_2[IO_2F_2][HF_2]$ and calculated metric parameters for gas-phase $IO_2F_2^-$

	Experimental	Calculated			Experimental
		MP2	SVWN		
Bond lengths and contacts (Å)					
I(1)–O(1)	1.774(2)	1.802	1.825	N(1)–C(1)	1.500(4)
I(1)–F(1)	2.025(2)	2.079	2.077	N(1)–C(2)	1.493(4)
I(1)–F(2)	2.027(2)			N(1)–C(3)	1.495(3)
F(3)···F(3A)	2.277(5)			N(2)–C(4)	1.500(4)
I(1)···F(3)	2.806(2)			N(2)–C(5)	1.488(4)
				N(2)–C(6)	1.499(3)
Bond angles (°)					
O(1)–I(1)–O(1A)	101.98(12)	109.11	109.84	C(1)–N(1)–C(2)	110.1(3)
O(1)–I(1)–F(1)	91.01(7)	94.27	93.08	C(1)–N(1)–C(3)	109.4(2)
O(1)–I(1)–F(2)	91.00(7)			C(2)–N(1)–C(3)	109.3(2)
F(1)–I(1)–F(2)	176.73(8)	165.24	169.26	C(4)–N(2)–C(5)	110.0(3)
F(3)···I(1)···F(3A)	84.63(8)			C(4)–N(2)–C(6)	109.5(2)
				C(5)–N(2)–C(6)	109.6(2)

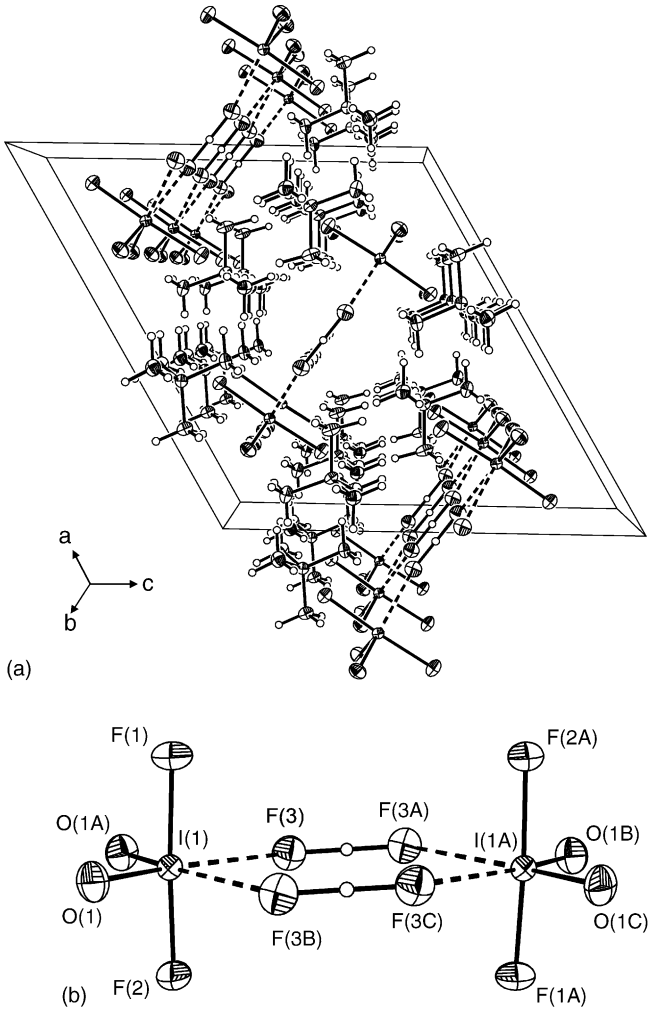

Fig. 3. View of (a) the $[N(CH_3)_4]_2[IO_2F_2][HF_2]$ unit cell showing the packing along the *b*-axis and (b) the $(IO_2F_2^-HF_2^-)_2$ structural unit; thermal ellipsoids are drawn at the 50% probability level.

coordination sphere of iodine to a pseudo-octahedron has been found in the crystal structure of $[K][IO_2F_2]$ [7] where two oxygen atoms from two adjacent $IO_2F_2^-$ anions form short contacts with the iodine atom (2.876(8), 2.887(12) Å; sum of the oxygen and iodine van der Waal's radii: 3.50 [30] and 3.55 Å [31]), which are, however, significantly longer than the I···F contacts in the $[N(CH_3)_4]_2[IO_2F_2][HF_2]$. A similar pseudo-octahedral coordination environment has also been found for Xe^{VI} in the crystal structure of XeO_2F_2 [19]. To the authors' knowledge, the symmetric bifluoride bridge in $[N(CH_3)_4]_2[IO_2F_2][HF_2]$ is unprecedented.

2.5. Computational results

The geometry of the $IO_2F_2^-$ anion was fully optimized and the vibrational frequencies were calculated at the MP2 and SVWN levels of theory. The calculated bond lengths and angles and vibrational frequencies are given in Tables 1 and 4, respectively. The bond lengths and angles calculated for the gas-phase $IO_2F_2^-$ anion are in good agreement with the X-ray crystallographic data in spite of the additional I···F contacts between the $IO_2F_2^-$ and HF_2^- in $[N(CH_3)_4]_2[IO_2F_2][HF_2]$. The vibrational frequencies obtained from the SVWN calculations show better agreement with the experimental frequencies than those at the MP2 level, which also does not reproduce the ordering of the symmetric and antisymmetric IO_2 stretches. Both levels of theory predict the reverse ordering of the symmetric and antisymmetric IF_2 stretches. The assignments of these experimental bands are based on the observed and calculated intensities. Attempts to obtain an energy-minimized gas-phase geometry for $[F_2O_2I(FHF)_2IO_2F_2]^{4-}$ at the MP2 level of theory failed, whereas a non-optimized geometry with two imaginary frequencies was obtained at the SVWN level. Apparently, the presence of counter-cations in the solid state is necessary to stabilize the quadruply charged anion.

3. Conclusion

The anhydrous $N(CH_3)_4^+$ salt of the $IO_2F_2^-$ anion was prepared and its Raman and infrared spectra were assigned with the aid of quantum mechanical calculations. The crystal structure of $[N(CH_3)_4]_2[IO_2F_2][HF_2]$ provides an unique example of bridging HF_2^- anions and more precise structural parameters for the $IO_2F_2^-$ anion than those are available from the crystal structure of $[K][IO_2F_2]$, enabling comparison of its geometric parameters with those of the isoelectronic XeO_2F_2 molecule. As in the cases of XeO_2F_2 and $XeO_2(OTeF_5)_2$, the axial fluorine ligands in the $IO_2F_2^-$ anion were found to be displaced towards the lone pair.

4. Experimental

4.1. Materials and apparatus

All volatile materials were handled on a Pyrex vacuum line equipped with glass/Teflon J. Young valves. Nonvolatile materials were handled in the dry nitrogen atmosphere of a dry box.

Acetonitrile solvent (Baker, HPLC Grade) was purified according to the standard literature method [32]. The syntheses of $[N(CH_3)_4][F]$ [15] and $[N(CH_3)_4][cis\text{-}IO_2F_4]$ [14] have been described previously.

4.2. Preparation of $[N(CH_3)_4][IO_3]$

Tetramethyl ammonium iodate was prepared by neutralization of an aqueous solution (ca. 7.5 mL) containing 3.502 g (19.32 mmol) of $[N(CH_3)_4][OH]\cdot 5H_2O$ (Fluka, $\geq$95.0%) with the same volume of an aqueous solution containing 3.399 g (19.32 mmol) of HIO_3 (BDH). The resulting solution was allowed to slowly evaporate to near dryness in the atmosphere. Removal of residual water under dynamic vacuum, followed by grinding and continued pumping at 50 °C, yielded 4.774 g (19.17 mmol, 99.22% yield) of $[N(CH_3)_4][IO_3]$.

4.3. Preparation of $[N(CH_3)_4][IO_2F_2]$

Approximately 1.8 mL of aqueous HF (49%, Fisher Scientific) was added to 0.408 g (1.64 mmol) of $[N(CH_3)_4][IO_3]$ contained in a 0.75 in. o.d. FEP vessel equipped with a stainless steel Whitey valve, yielding a colorless solution. Water and HF were slowly removed under dynamic vacuum at room temperature. The resulting white solid was further dried under dynamic vacuum at 80 °C for 2 h.

4.4. Crystal growth of $[N(CH_3)_4]_2[IO_2F_2][HF_2]$

The white solid obtained from the extraction of a $[N(CH_3)_4]_2[IO_2F_5]/[N(CH_3)_4][cis\text{-}IO_2F_4]$ mixture using CH_3CN [14] was used for crystal growth. Approximately 6 mL of CH_3CN was distilled onto the solid in one arm of an evacuated H-shaped reactor constructed from 12 mm o.d. glass tubing and equipped with a J. Young valve, followed by dissolution of the solid at 50 °C after backfilling the reactor with 1 atm of dry nitrogen gas. The side arm containing the solution was placed inside a glass Dewar containing water at 50 °C, covered with a styroform lid, and was allowed to cool to room temperature over a period of 4 days. Most of the solvent condensed into the other side arm and several colorless, needle-shaped crystals grew above the solvent level in the arm containing the solution. The majority of the supernatant remaining above the crystals was removed with a pipette inside a dry nitrogen-filled glove bag followed by pumping off the residual CH_3CN on a glass vacuum line for 1 min. Crystals were mounted in 0.1 mm glass Lindemann capillaries inside the dry box, plugged with Kel-F wax and heat-sealed with a micro-torch outside the dry box. The colorless, needle-shaped crystal used for X-ray data collection had the dimensions 0.8 mm × 0.02 mm × 0.08 mm.

4.5. X-ray structure determination

4.5.1. Collection and reduction of X-ray data

X-ray diffraction data were collected using a P4 Siemens diffractometer equipped with a Siemens SMART 1K charge-coupled device (CCD) area detector (by use of the program SMART) [33] and a rotating anode (graphite-monochromated Mo Kα radiation, λ = 0.71073 Å). The crystal-to-detector distance was 3.9910 cm and the data collection was carried out in 512 × 512 pixel mode using 2 × 2 pixel binning. A complete sphere of data was collected to better than 0.8 Å resolution. Processing was carried out by using the program SAINT [33], which applied Lorentz and polarization corrections to three-dimensionally integrated diffraction spots. The program SADABS [34] was used for the scaling of diffraction data, the application of a decay correction and an empirical absorption correction based on redundant reflections.

4.5.2. Solution and refinement of the structure

All calculations were performed using the SHELXTL Plus package [35] for structure determination, refinement and molecular graphics.

The XPREP program [35] was used to confirm the unit cell dimensions and the crystal lattice. A solution was obtained using direct methods which located the positions of the iodine atoms. Successive difference Fourier syntheses revealed all light atoms, which were assigned on the basis of their bond distances to the heavy atoms. The final refinement was obtained by introducing a weighting factor and anisotropic thermal parameters for all non-hydrogen atoms, giving a residual, R_1, of 0.0192 (wR_2 = 0.0455) and maximum and minimum electron densities in the final difference Fourier map of 0.680/−0.561. The residual

electron densities were located around the iodine atoms. The hydrogen atoms were refined isotropically.

4.6. Raman spectroscopy

The Raman spectrum of $[N(CH_3)_4][IO_2F_2]$ was recorded on a Bruker RFS 100 FT Raman spectrometer with a quartz beam splitter, a liquid-nitrogen-cooled Ge detector, and a low-temperature accessory. The 1064 nm line of an Nd:YAG laser was used for excitation of the sample. The backscattered (180°) radiation was sampled. The actual usable Stokes range was 50–3500 cm^{-1} with a spectral resolution of 1 cm^{-1}. The low-temperature spectrum of $[N(CH_3)_4][IO_2F_2]$ was recorded on a powdered sample in a melting point capillary using a laser power of 200 mW. The Raman spectrum of $[N(CH_3)_4]_2[IO_2F_2][HF_2]$ was excited using the 514.5 nm line of a Ar ion laser and was recorded on a Jobin-Yvon Mole S-3000 triple spectrograph system as previously described [36]. An Olympus metallurgical microscope (model BHSM-L-2) was used for focusing the excitation laser to a 1-μm spot on a single crystal of $[N(CH_3)_4]_2[IO_2F_2][HF_2]$ in a dry Lindemann capillary at room temperature.

4.7. Infrared spectroscopy

The FT-infrared spectrum of $[N(CH_3)_4][IO_2F_2]$ was recorded on a Nicolet Avatar 360 FTIR spectrometer at ambient temperature. An AgCl pellet was formed in a Wilks minipress inside the dry box by sandwiching the sample between two layers of AgCl disks. The spectra were acquired in 64 scans at a resolution of 2 cm^{-1}.

4.8. NMR spectroscopy

The ^{19}F NMR spectrum (235.35 MHz) of $[N(CH_3)_4][IO_2F_2]$ in CH_3CN solvent was recorded unlocked on a Bruker AC-250 spectrometer equipped with a Tecmag console and a dual 5-mm $^{1}H/^{13}C$ probe and referenced to external $CFCl_3$. The spectrum was acquired, with no relaxation delay, in a 64 K memory using a spectral width setting of 60 kHz, yielding an acquisition time of 1.09 s and data point resolution of 0.92 Hz/data point. A total of 72 transients were acquired.

4.9. Calculations

Electronic structure calculations were carried out at the Møller-Plesset perturbation level with correction for electron correlation to the second order (MP2) and local spin density exchange and Vosko, Wilk, and Nusair 1980 correlation functional (SVWN) levels of theory as implemented in the program Gaussian-98 (version A-11) [37]. Stuttgart relativistic large core (RLC) effective core pseudopotential (ECP) basis sets [38,39], augmented with two Huzinaga d-polarization functions [40], were used for MP2 calculations, while double zeta valence polarization (DZVP) basis sets [41,42] optimized for density functional calculations were used for the SVWN calculations.

5. Supplementary materials

Crystallographic data for the structure in this paper have been deposited with the Fachinformationzentrum Karlsruhe (FIZ) as supplementary publication No. CSD 414126. Copies of the data can be obtained, free of charge, on application to FIZ, abt. PROKA, 76344 Eggenstein-Leopoldshafen, Germany (Tel.: +49 7247 808 205 or e-mail: crysdata@fiz-karlsruhe.de).

Acknowledgements

We thank the donors of the Petroleum Research Fund, administered by the American Chemical Society, for support of this work under ACS-PRF No. 37128-AC3 (G.J.S.) as well as the Natural Sciences and Engineering Research Council of Canada (M.G. and G.J.S.), and the University of Lethbridge (M.G.) for support of this work. We also thank Prof. F. Aubke, University of British Columbia, for his donation of AgCl sheet used in this work.

References

[1] H. Selig, U. Elgad, in: J.J. Katz, I. Sheft (Eds.), Herbert H. Hyman Memorial Volume, J. Inorg. Nucl. Chem. Suppl., Pergaman Press Ltd., Oxford, England, 1976, pp. 91–94.
[2] K.O. Christe, R.D. Wilson, C.J. Schack, Inorg. Chem. 20 (1981) 2104–2114.
[3] H. Selig, U. El-Gad, J. Inorg. Nucl. Chem. 35 (1973) 3517–3522.
[4] R.F. Weinland, O. Lauenstein, Z. Anorg, Allg. Chem. 20 (1899) 30–39.
[5] J.B. Milne, D.M. Moffett, Inorg. Chem. 15 (1976) 2165–2169.
[6] J.J. Pitts, S. Kongpricha, A.W. Jache, Inorg. Chem. 4 (1965) 257–259.
[7] L. Helmholz, M.T. Rogers, J. Am. Chem. Soc. 62 (1940) 1537–1542.
[8] S.C. Abrahams, J.L. Bernstein, J. Chem. Phys. 64 (1976) 3254–3260.
[9] H.A. Carter, F. Aubke, Inorg. Chem. 10 (1971) 2296–2301.
[10] A. Finch, P.N. Gates, M.A. Jenkinson, J. Fluorine Chem. 2 (1972) 111–112.
[11] J.B. Milne, D. Moffett, Inorg. Chem. 14 (1975) 1077–1081.
[12] M. Gerken, J.P. Mack, Unpublished results.
[13] K.O. Christe, W.W. Wilson, R.D. Wilson, Inorg. Chem. 28 (1989) 904–908.
[14] J.A. Boatz, K.O. Christe, D.A. Dixon, B.A. Fir, M. Gerken, R.Z. Gnann, H.P.A. Mercier, G.J. Schrobilgen, Inorg. Chem. 42 (2003) 5282–5292.
[15] K.O. Christe, W.W. Wilson, R.D. Wilson, R. Bau, J.-A. Feng, J. Am. Chem. Soc. 112 (1990) 7619–7625.
[16] G. Kabisch, J. Raman Spectrosc. 9 (1980) 279–285.
[17] W.W. Wilson, K.O. Christe, J.-A. Feng, R. Bau, Can. J. Chem. 67 (1989) 1898–1901.
[18] R.J. Gillespie, I. Hargittai, The VSEPR Model of Molecular Geometry, Allyn and Bacon, Boston, MA, 1991.
[19] S.W. Peterson, R.D. Willet, J.L. Huston, J. Chem. Phys. 59 (1973) 453–459.

[20] N. LeBlond, D.A. Dixon, G.J. Schrobilgen, Inorg. Chem. 39 (2000) 2473–2487.
[21] L. Turowsky, K. Seppelt, Z. Anorg. Allg. Chem. 609 (1992) 153–156.
[22] R.J. Gillespie, E.A. Robinson, Angew. Chem. 108 (1996) 539–560;
R.J. Gillespie, E.A. Robinson, Angew. Chem., Int. Ed. Engl. 35 (1996) 495–514.
[23] T. Braun, S.P. Foxon, R.N. Perutz, P.H. Walton, Angew. Chem. 111 (1999) 3543–3599;
T. Braun, S.P. Foxon, R.N. Perutz, P.H. Walton, Angew. Chem., Int. Ed. Engl. 38 (1999) 3326–3328.
[24] V.J. Murphy, T. Hascall, J.Y. Chen, G. Parkin, J. Am. Chem. Soc. 118 (1996) 7428–7429.
[25] V.J. Murphy, D. Rabinovich, T. Hascall, W.T. Klooster, T.F. Koetzle, G. Parkin, J. Am. Chem. Soc. 120 (1998) 4372–4387.
[26] D.C. Roe, W.J. Marshall, F. Davidson, P.D. Soper, V.V. Grushin, Organometallics 19 (2000) 4575–4582.
[27] M.K. Whittlesey, R.N. Perutz, B. Greener, M.H. Moore, J. Chem. Soc., Chem. Commun. (1997) 187–188.
[28] H.W. Roesky, M. Sotoodeh, Y.M. Xu, F. Schrumpf, M. Noltemeyer, Z. Anorg, Allg. Chem. 580 (1990) 131–138.
[29] M. Gerken, D.A. Dixon, G.J. Schrobilgen, Inorg. Chem. 41 (2002) 259–277.
[30] A. Bondi, J. Phys. Chem. 68 (1964) 441–451.
[31] L. Pauling, The Nature of the Chemical Bond, 3rd ed. Cornell University Press, Ithaca, NY, 1960, p. 260.
[32] J.M. Winfield, J. Fluorine Chem. 25 (1984) 91–98.
[33] SMART and SAINT, Release 4.05, Siemens Energy and Automation, Inc., Madison, WI, 1996.
[34] G.M. Sheldrick, SADABS (Siemens Area Detector Absorption Corrections), Personal communication, 1996.
[35] G.M. Sheldrick, SHELXTL-Plus Release 5.03, Siemens Analytical X-ray Instruments, Inc., Madison, WI, 1994.
[36] W.J. Casteel Jr., P. Kolb, N. LeBlond, H.P.A. Mercier, G.J. Schrobilgen, Inorg. Chem. 35 (1996) 929–942.
[37] M.J. Frisch, G.W. Trucks, H.B. Schlegel, G.E. Scuseria, M.A. Robb, J.R. Cheeseman, V.G. Zakrzewski, J.A. Montgomery Jr., R.E. Stratmann, J.C. Burant, S. Dapprich, J.M. Millam, A.D. Daniels, K.N. Kudin, M.C. Strain, O. Farkas, J. Tomasi, V. Barone, M. Cossi, R. Cammi, B. Mennucci, C. Pomelli, C. Adamo, S. Clifford, J. Ochterski, G.A. Petersson, P.Y. Ayala, Q. Cui, K. Morokuma, P. Salvador, J.J. Dannenberg, D.K. Malick, A.D. Rabuck, K. Raghavachari, J.B. Foresman, J. Cioslowski, J.V. Ortiz, A.G. Baboul, B.B. Stefanov, G. Liu, A. Liashenko, P. Piskorz, I. Komaromi, R. Gomperts, R.L. Martin, D.J. Fox, T. Keith, M.A. Al-Laham, C.Y. Peng, A. Nanayakkara, M. Challacombe, P.M.W. Gill, B. Johnson, W. Chen, M.W. Wong, J.L. Andres, C. Gonzalez, M. Head-Gordon, E.S. Replogle, J.A. Pople, Gaussian-98, Revision A.11, Gaussian, Inc., Pittsburgh, PA, 2001.
[38] G. Igel-Mann, H. Stoll, H. Preuss, Mol. Phys. 65 (1988) 1321–1328.
[39] W. Kuechle, M. Dolg, H. Stoll, H. Preuss, Mol. Phys. 74 (1991) 1245–1263.
[40] S. Huzinaga, J. Andzelm, M. Klobukowski, E. Radzio-Andzelm, Y. Sakai, H. Tatewaki, Gaussian basis sets for molecular calculations, in: Physical Science Data, vol. 16, Elsevier, Amsterdam, 1984.
[41] N. Godbout, D.R. Salahub, J. Andzelm, E. Wimmer, Can. J. Chem. 70 (1992) 560–571.
[42] C. Sosa, J. Andzelm, B.C. Elkin, E. Wimmer, K.D. Dobbs, D.A. Dixon, J. Phys. Chem. 96 (1992) 6630–6636.